ACS Catalysis

NOVEMBER 2018 VOLUME 8 NUMBER 11 PUBS.ACS.ORG/ACSCATALYSIS

ACS Publications
Most Trusted. Most Cited. Most Read.

www.acs.org

ACS Catalysis

Research Article

Cite This: ACS Catal. 2018, 8, 9992−10003

pubs.acs.org/acscatalysis

Mechanistic Insights into Interactions between Bacterial Class I P450 Enzymes and Redox Partners

Wei Zhang,[§,‡,†] Lei Du,[‡,†] Fengwei Li,[‡] Xingwang Zhang,[‡] Zepeng Qu,[‡,⊥] Lei Han,[ξ] Zhong Li,[‡,⊥] Jingran Sun,[‡] Fengxia Qi,[‡] Qiuping Yao,[‡] Yue Sun,[‡] Ce Geng,[‡] and Shengying Li*[,‡,⊥]

[§]State Key Laboratory of Microbial Technology, Shandong University, Qingdao, Shandong 266237, China

[‡]Shandong Provincial Key Laboratory of Synthetic Biology, CAS Key Laboratory of Biofuels, Qingdao Institute of Bioenergy and Bioprocess Technology, Chinese Academy of Sciences, No. 189 Songling Road, Qingdao, Shandong 266101, China

[⊥]University of Chinese Academy of Sciences, No. 19(A) Yuquan Road, Beijing 100049, China

[ξ]College of Chemistry and Pharmaceutical Sciences, Qingdao Agricultural University, Qingdao, Shandong 266109, China

Supporting Information

ABSTRACT: Cytochrome P450 enzymes are highly diversified biocatalysts associated with steroid biosynthesis, xenobiotic metabolism, biosynthesis of natural products, and industrial oxidation reactions. A typical P450 catalytic cycle requires sequential transfer of two electrons from NAD(P)H to the heme-iron reactive center for O_2 activation. For the most abundant bacterial Class I P450 systems, this important process is usually mediated by two redox partner proteins including an FAD-containing ferredoxin reductase (FdR) and a small iron−sulfur protein, ferredoxin (Fdx). However, it is often unclear which pair of Fdx and FdR among multiple redox partners is the optimal one for a specific Class I P450 enzyme. To address this important but underexplored question, herein, a reaction matrix network with 16 Fdxs, 8 FdRs, and 6 P450s (against 7 substrates) was constituted. By analyzing the reactivity profiles of 896 P450 reactions, together with phylogenetic analysis, redox potential measurements, structural simulations, and Fdx-P450 molecular docking, we provide important mechanistic insights into the recognition and interactions between bacterial Class I P450 enzymes and redox partners.

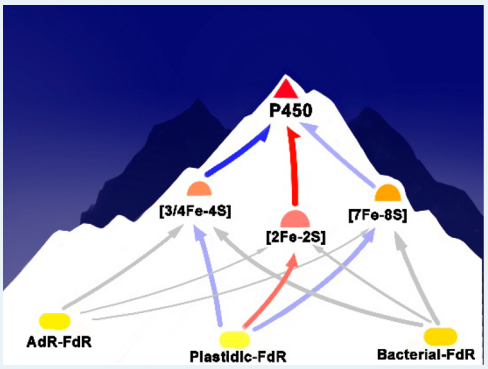

KEYWORDS: *cytochrome P450 enzymes, redox partners, electron transfer, protein−protein interaction, ferredoxin, ferredoxin reductase*

INTRODUCTION

Ubiquitous cytochrome P450 enzymes (P450s or CYPs) form a superfamily of heme-containing biocatalysts with tremendous diversity and functional versatility.[1,2] In nature, CYPs catalyze numerous reactions that are involved in steroid biosynthesis, xenobiotic metabolism, and biosynthesis of diverse natural products.[1,3,4] For biotechnological applications, P450s are useful metalloenzymes to mediate regio- and stereoselective oxidation of diverse substrates.[5,6] Most CYPs require two electrons shuttled from NAD(P)H to the heme-iron catalytic center by redox partner proteins to generate reactive species.[4] With some exceptions,[7] there are two major classes of redox partner systems. For the most abundant Class I P450 enzymes including most bacterial and mitochondrial P450s, their redox partner systems consist of a small iron−sulfur ferredoxin (Fdx) and an FAD-containing ferredoxin reductase (FdR), forming the electron transport pathway of NAD(P)H → FdR → Fdx → P450. By contrast, the eukaryotic membrane-bound Class II P450s normally recruit a single FAD/FMN-containing flavoprotein that is referred to as cytochrome P450 reductase (CPR) to shuttle reducing equivalents.

In the pregenomic era, the natural redox partners of bacterial P450s were mostly unknown. Thus, practically, surrogate redox partners, such as spinach Fdx/FdR, bovine adrenodoxin (Adx)/adrenodoxin reductase (AdR), putidaredoxin (Pdx)/putidaredoxin reductase (PdR) from *Pseudomonas putida*, and the RhFRED reductase domain from *Rhodococcus* sp., acting either in separation or as artificially fused proteins, have been widely used in reconstitution of P450 activities both in vitro and in vivo[7−10] However, the use of these heterologous redox partners sometimes may fail or often compromise the P450 catalytic activities[7,11] which are crucial for synthetic applications of CYPs.

In the current postgenomic era, the explosive genome sequencing data have revealed that, unlike eukaryotes whose genome usually contains a single (sometimes two) CPR-encoding gene(s),[12] bacterial genomes often have a larger number of genes that encode multiple Fdxs and FdRs. For example, *Streptomyces coelicolor* A3(2) has six Fdx genes and four FdR genes;[13] *Corynebacterium glutamicum* ATCC 13032 possesses three Fdx genes and three FdR genes;[14] and the

Received: July 24, 2018
Revised: September 10, 2018
Published: September 28, 2018

DOI: 10.1021/acscatal.8b02913
ACS Catal. 2018, 8, 9992−10003

Scheme 1. Reactions Catalyzed by (A) MycG, (B) PikC, (C) CreJ, (D) $P450_{cam}$, and (E) CYP105AS-1 and P450sca2[a]

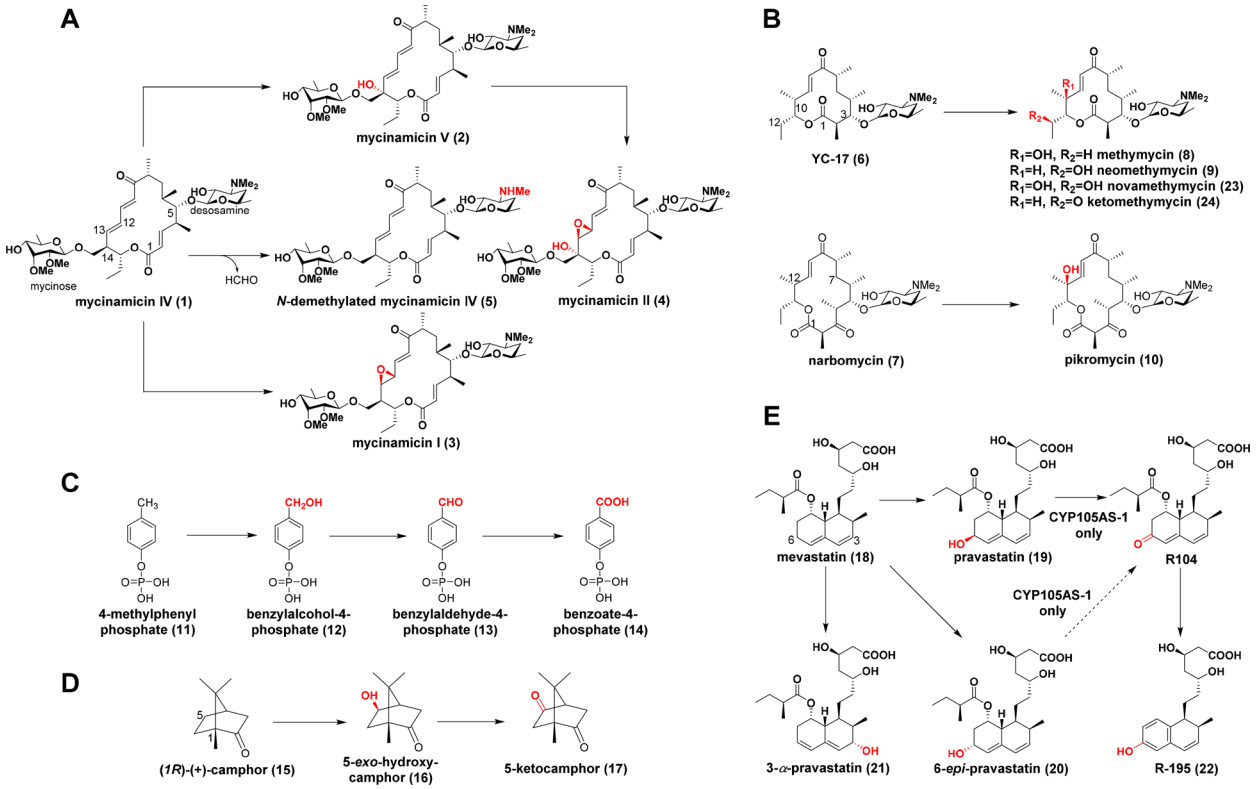

[a]The oxidative functional groups installed by P450s are colored in red.

cyanobacterium *Synechococcus elongatus* PCC 7942 holds seven Fdx genes and one FdR gene.[15] Notably, microorganisms have evolved distinct types of Fdxs and FdRs (Tables S1 and S2), and these redox proteins can serve many different physiological processes.[16−18] Thus, it is often unclear which pair of Fdx and FdR is the optimal redox partner proteins for a specific bacterial Class I P450 enzyme unless their coding genes and the P450 gene exist in the same operon;[19] even so, it remains unproven whether these cotranscribed redox partner genes necessarily encode the best Fdx/FdR pairs for their neighboring CYPs.

Surprisingly, few studies[7,20−24] have been carried out to address the above and the following important questions about the functional pairing between prokaryotic Class I P450s and redox partners, either homologously or heterologously: (1) Are there any P450 preferred types of Fdx and FdR in microorganisms? (2) If yes, what are the recognizing factors of the P450-specific Fdx and FdR? (3) Are there any general principles to guide the selection of appropriate redox partners to support a certain P450 enzyme? To resolve these problems that were previously underexplored, in this study, we chose six bacterial Class I P450 enzymes, including $P450_{cam}$ (CYP101A1) from *P. putida*, MycG (CYP107E1) from *Micromonospora griseorubida*, PikC (CYP107L1) from *S. venezuelae*, CreJ (CYP288A2) from *C. glutamicum*, CYP105AS-1 from *Amycolatopsis orientalis*, and P450sca2 (CYP105A3) from *S. carbophilus*, to constitute a reaction matrix network with 16 Fdxs and 8 FdRs (Tables S1 and S2), which represent the full sets of Fdx/FdR from *S. coelicolor* A3(2),[13] *S. elongatus* PCC 7942,[15] and *C. glutamicum* ATCC 13032.[14] By analyzing the reactivity profiles (substrate conversions and product distributions) of 896 P450 reactions, together with phylogenetic analysis, redox potential measurements, structural simulations, and Fdx-P450 molecular docking, we provide new mechanistic insights into interactions between bacterial Class I P450 enzymes and redox partners.

RESULTS

Among the selected P450s, the multifunctional P450 enzyme MycG is responsible for the C14 hydroxylation and the C12═C13 epoxidation of the 16-membered ring macrolide antibiotic mycinamicin IV (**1**), giving rise to mycinamicin V (**2**) and mycinamicin I (**3**), respectively. MycG epoxidizes **2** to the final product mycinamicin II (**4**), while it cannot further modify **3**.[25−27] Moreover, we recently reported that MycG is also able to catalyze the unnatural *N*-demethylation of **1** when partnered with the isolated RhFRED, yielding *N*-demethylated mycinamicin IV (**5**)[28] (Scheme 1A). PikC with innate substrate flexibility has two natural substrates including the 12-membered ring macrolide YC-17 (**6**) and the 14-membered ring macrolide narbomycin (**7**).[8] Physiologically, PikC hydroxylates **6** at either C10 or C12 almost equally, yielding methymycin (**8**) and neomethymycin (**9**), respectively. The hydroxylation of **7** by PikC predominantly occurs at C12, leading to the production of pikromycin (**10**) (Scheme 1B).[29] CreJ is the central biocatalyst of the 4-cresol biodegradation pathway.[14] Supported by its cognate redox partners *Cgl*Fdx0526 (i.e., CreF) and *Cgl*FdR0525 (i.e., CreE), this catabolic P450 enzyme is capable of successively oxidizing 4-methylphenyl phosphate (**11**, the activated form of 4-cresol) to benzylalcohol-4-phosphate (**12**), benzylaldehyde-4-phosphate (**13**), and benzoate-4-phosphate (**14**) (Scheme 1C). The prototypical $P450_{cam}$ selectively converts (1*R*)-(+)-camphor (**15**) into 5-*exo*-hydroxy-camphor (**16**)[30] and further to 5-ketocamphor (**17**) (Scheme 1D).[31] With regard to CYP105AS-1 and P450sca2, both P450 enzymes catalyze the

DOI: 10.1021/acscatal.8b02913
ACS Catal. 2018, 8, 9992−10003

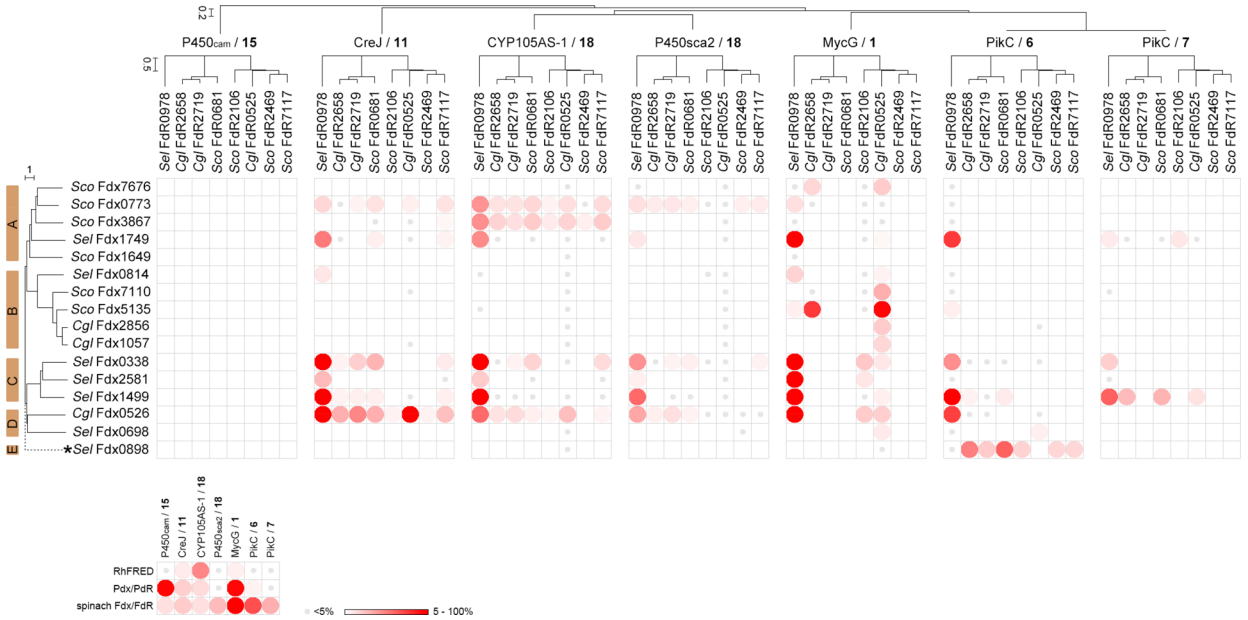

Figure 1. P450 reaction matrix network (upper panel) formed by 6 bacterial P450 enzymes (against 7 substrates), 16 Fdxs, and 8 FdRs, whose phylogenetic trees are displayed aside. The reference reactions are shown in the lower panel. The intensities of red colors indicate the differential substrate conversion ratios. Abbreviations: *Sco*, *Streptomyces coelicolor*; *Sel*: *Synechococcus elongates*; *Cgl*: *Corynebacterium glutamicum*. The asterisk represents the unique thioredoxin-like *Sel*Fdx0898 that is arbitrarily assigned as Branch E.

oxidation of mevastatin (**18**) to pravastatin (**19**), 6-*epi*-pravastatin (**20**), and 3-α-pravastatin (**21**) to various extents (Scheme 1E).[10,32]

To constitute a systematic P450 reaction matrix network, each individual P450 reaction was in vitro carried out using 128 (16 × 8) different Fdx/FdR combinations, in the presence of NADPH. Spinach Fdx/FdR, Pdx/PdR, and the stand-alone form of RhFRED were used as references. As shown in Figure 1 (see Tables S3−S16 for detailed data), seven kinds of reactions catalyzed by six P450 enzymes showed distinct reactivity patterns. It is worth noting that the use of NADPH or NADH generated similar reactivity patterns (data not shown) although the sequence analysis suggests different cofactor preference of the eight FdRs (Table S2, Figure S1), indicating that the transfer of hydride ion from NAD(P)H to FdR is not the rate-limiting step under our reaction conditions (see the Supporting Information). The positive reaction percentages of seven matrices ranged from 0 to 42.2% (0−22.6% if only counting the reactions with the substrate conversion ratios higher than 5%, the same below), with $P450_{cam}$ and CYP105AS-1 being the tested P450s with the lowest and the highest redox partner flexibility. *Cgl*Fdx0526 turned out to be the Fdx with the widest spectrum of activities, which supported 53.6% (41.4%) of the tested reactions. Interestingly, *Cgl*Fdx0526 and the other two wide-spectrum Fdxs including *Sel*Fdx1499 and *Sel*Fdx0338 are all Fe_2S_2 ferredoxins. Although the Fe_3S_4 ferredoxin *Sco*Fdx0773 also showed activities in a significant portion of reactions, it was not able to support the two sets of PikC reactions. As the most flexible FdRs, *Sel*FdR0978 and *Cgl*FdR0525 were able to support 45.5% (31.2%) and 49.1% (16.1%) of tested reactions, respectively.

Importantly, in addition to the reference redox partners, only 4 out of 128 pairs of redox partners including *Sel*Fdx1749/*Sel*FdR0978, *Sel*Fdx0338/*Sel*FdR0978, *Sel*Fdx2581/*Sel*FdR0978, and *Sel*Fdx1499/*Sel*FdR0978 were active in all P450 reactions except for the highly specific $P450_{cam}$ reactions, with the final pair being optimal in terms of overall substrate conversions. Remarkably, there was not an Fdx or an FdR that is totally inactive in all reactions, indicating that all used redox partners are functional proteins.

Specifically, none of the 128 tested redox partner combinations gave a detectable product for **15** oxidation by $P450_{cam}$ (Figure 1, Table S3), while the cognate redox partners Pdx/PdR supported the reaction with 96.2% substrate conversion. By contrast, spinach Fdx/FdR and RhFRED only showed marginal supporting activity toward $P450_{cam}$ (Table S10). These results are consistent with previous studies indicating that the interaction between Pdx and $P450_{cam}$ is highly specific.[33,34] In addition to the normal electron transfer role, Pdx also serves as an effector to induce the productive structural change of $P450_{cam}$.

*Cgl*Fdx0526 and *Cgl*FdR0525 are considered cognate redox partner proteins for CreJ since their coding genes are located within the same operon.[35−37] This native combination led to 97.7% conversion of **11**, while *Cgl*Fdx1057/*Cgl*FdR0525 and *Cgl*Fdx2856/*Cgl*FdR0525 from the same host bacterium only resulted in approximately 3.1% and negligible level of **11** consumption, respectively (Table S4). The eight tested FdRs all generated positive reactions when coupled with *Cgl*Fdx0526 (Figure 1). When partnered with *Cgl*FdR0525, only 43.8% (12.5%) of Fdxs gave positive results, suggesting that Fdx is likely a more important factor than FdR with respect to reconstitution of an active P450 reaction system. This is unsurprising because Fdx instead of FdR directly interacts with the P450 enzyme. Interestingly, the hybrid group of *Cgl*Fdx0526/*Sel*FdR0978 and the heterologous groups of *Sel*Fdx0338/*Sel*FdR0978 and *Sel*Fdx1499/*Sel*FdR0978 led to complete substrate conversions, which suggests surrogate redox partners could be superior to the cognate ones. Regarding the products distribution, the alcohol product **12** was observed to be the main product with fluctuated yields in all positive reactions (Table S11).

DOI: 10.1021/acscatal.8b02913
ACS Catal. 2018, 8, 9992−10003

CYP105AS-1 and P450sca2 (CYP105A3), which are 28.5%/41.2% identical/similar to each other, share the common functionality of hydroxylating **18** to **19**–**21**.[10,32] Since compound **19** is a clinic drug to lower the cholesterol level, the biotransformation from **18** to **19** has great industrial significance.[38] The reactivity patterns of these two CYP105 family members are quite similar (Figure 1), suggesting a possible correlation between protein sequence similarity, P450 functionality, and the selectivity toward redox partners. Among the 128 reactions, 42.2% (22.6%) and 32.0% (13.3%) of Fdx/FdR combinations supported the activity of CYP105AS-1 and P450sca2, respectively (Tables S5 and S6). The lower positive ratio of P450sca2 is mainly because of the differential behaviors of *Sco*Fdx3867, which specifically supported the activity of CYP105AS-1 for unknown reasons. When *Sel*FdR0978 was coupled with *Sel*Fdx0338 or *Sel*Fdx1499, the conversion rates of **18** by CYP105AS-1 reached 99.6% and 98.2%, respectively (Table S5), while the corresponding percentage numbers for P450sca2 were 42.7% and 58.2% (Table S6). Overall, the catalytic efficiencies of CYP105AS-1 were almost always higher than those of P450sca2 when they were incubated with the same pairs of Fdx/FdR. These results might be explained, at least in part, by the large difference in the midpoint redox potentials of these two P450s with substrate bound (−130 mV for CYP105AS-1 vs −253 mV for P450sca2, Table 1) because a P450 enzyme with higher redox potential is more inclined to accept electrons from an Fdx with more negative redox potential.[39]

Table 1. Midpoint Redox Potential Values of the Studied P450s in the Presence and Absence of Corresponding Substrates

enzyme	substrate	midpoint redox potential (mV)
MycG	–	−175
MycG	**1**	−92
PikC	–	−123
PikC	**6**	−85
PikC	**7**	−110
CreJ	–	−147
CreJ	**11**	−133
$P450_{cam}$	–	−289
$P450_{cam}$	**15**	−154
CYP105AS-1	–	−129
CYP105AS-1	**18**	−130
P450sca2	–	−250
P450sca2	**18**	−253

Unlike P450sca2 that mainly produced **19** in all positive reactions, the main products of CYP105AS-1 were **20** and **21** in a majority of positive reactions (Tables S12 and S13). Strikingly, a new product (**22**) was observed when CYP105AS-1 was in companion with either *Sel*Fdx0338/*Sel*FdR0978 or *Sel*Fdx1499/*Sel*FdR0978 (Figure 2A, trace (ii) and (iii)) compared to RhFRED as a control,[32] which only led to the production of **20** and **21** (Figure 2A, trace (iv)). The structure was determined as R-195 by high-resolution mass spectrometry ($C_{18}H_{24}NO_5$, $[M + H]^+$: obsd 321.1703, calcd 321.1697) (Figure S2) and ^1H NMR analysis[40] (see the Supporting Information). This compound was previously reported to be a hepatic metabolite of **19** upon the 6-β-hydroxy-dehydrogenation activity of 3-hydroxysteroid dehydrogenase in rat hepatocytes.[41] It is the first time to observe **22** as a bioconversion product of a bacterial P450 system. Mechanistically, **19** and/or **20** could be further oxidized to the 6-keto intermediate R-104 (Scheme 1E), followed by spontaneous deesterification and aromatization, giving rise to **22**.

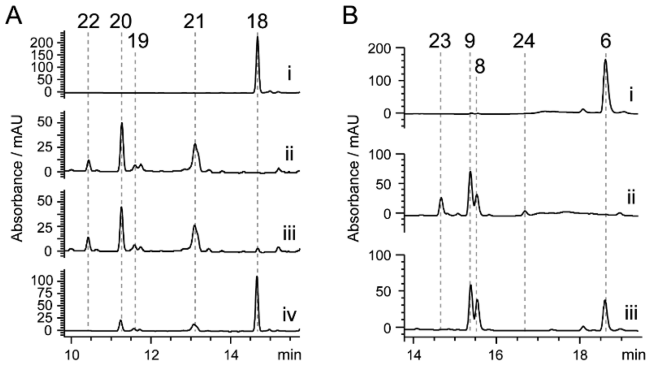

Figure 2. HPLC analysis (240 nm) of the representative oxidative reactions catalyzed by (A) CYP105AS-1 and (B) PikC when partnered with different Fdxs in the presence of *Sel*FdR0978 and NADPH. (A) (i) negative control, (ii) *Sel*Fdx0338, (iii) *Sel*Fdx1499, and (iv) the reference reaction using RhFRED as redox partner. (B) (i) negative control, (ii) *Sel*Fdx1499, and (iii) the reference reaction using spinach Fdx and FdR as redox partners.

For MycG, 31.2% (18.8%) of Fdx/FdR combinations were capable of supporting the oxidation of **1** with varying efficiencies that ranged from 0.5% to 99.6% (Table S7). The two ferredoxin reductases including *Sel*FdR0978 and *Cgl*FdR0525 demonstrated significantly broader spectra of activities than the rest of the FdRs. In particular, when *Sel*FdR0978 was coupled with *Sel*Fdx1749, *Sel*Fdx0338, *Sel*Fdx2581, *Sel*Fdx1499, or *Cgl*Fdx0526, >99.0% substrate conversion of **1** was achieved. For *Sel*FdR0978, the selection of different Fdxs led to a broad range of substrate conversion rates and different product distributions (Table S14), again indicating the important role of Fdx in modulating the activity of P450s. The main product was found to be the final product **4** in a majority of the *Sel*FdR0978 group of reactions, while the intermediate **2** was the dominant product in most cases when *Cgl*FdR0525 was used to source electrons from NAD(P)H. These results suggest that *Cgl*FdR0525 might not be as efficient as *Sel*FdR0978 in transferring electrons to support the MycG activity. It is noteworthy that no demethylated product was observed in all tested reactions, as previously identified when MycG was partnered by the stand-alone form of RhFRED or an engineered *Rhodococcus*-spinach hybrid RhFRED-Fdx reductase.[28]

PikC recognizes both **6** and **7** as natural substrates.[29,42,43] Surprisingly, the same P450 enzyme showed distinct reactivity patterns toward different substrates (Figure 1). When **6** was used as substrate, the ratio of positive redox partner combinations was 24.2% (10.9%), while the corresponding rate was only 9.4% (5.5%) for the PikC reaction using **7** as substrate (Tables S8 and S9). Specifically, *Cgl*Fdx0526 supported four (one) out of eight reactions of **6** but failed to reconstitute any reactions of **7**. These results illustrate that the substrate plays an important role in affecting the selectivity of P450 toward Fdx. We reason that the binding of different substrates might induce differential conformational changes of the interaction interface between P450 and Fdx. Indeed, some differences in conformation and charged surfaces can be seen on the proximal side of PikC upon binding of **6** or **7** (Figure S3). Moreover, it is well-known that the binding of substrate induces the shift of P450 redox potential to a more positive value, thereby favoring the electron transfer from Fdx to heme-iron.[44] Experimentally, the redox potential of **6**-bound PikC was 25 and 38 mV

DOI: 10.1021/acscatal.8b02913
ACS Catal. 2018, 8, 9992−10003

higher than those of **7**-bound and substrate-free PikC (−85 mV vs −110 mV vs −123 mV, Table 1), which may also partially explain why the **6**-bound form of PikC was able to work with more redox partners and showed higher activities than the PikC−**7** complex.

With regard to the product distributions of PikC/**6** reactions, the ratios between **8** and **9** ranged from 1:0.9 to 1:2.3 (Table S15). In particular, the combination of *Sel*Fdx1499 and *Sel*FdR0978 resulted in 48.6% conversion of **6** into four products including **8**, **9**, and two dioxygenation products **23** and **24** (Figure 2B, trace (ii), whose m/z values were measured to be 486.3072 ($C_{25}H_{43}NO_8$, $[M + H]^+$: calcd 486.3061) and 468.2958 ($C_{25}H_{41}NO_7$, $[M + H]^+$: calcd 468.2956) (Figure S4), respectively, under the positive ion mode by HRMS. The m/z value of **23** is 16 amu greater than that of **8** or **9**, suggesting a double-hydroxylation product, which was further identified as novamethymycin,[45] a known compound derived from **8**, based on analysis of its ^{1}H NMR spectrum[46] (see the Supporting Information). Similarly, compound **24** with the m/z value that is 2 amu less than that of **8** and **9** was identified as ketomethymycin by HRMS and ^{1}H NMR analysis[46] (see the Supporting Information). Notably, **24** was previously reported by Sherman and co-workers,[46] where it was proposed to stem from dihydroxylation of **6** at the C12 position and followed by spontaneous dehydration of the germinal diol intermediate. The production of **23** and **24** cannot be simply explained by overoxidation due to the higher efficiency of electron transfer, since no such dihydroxylated products were detected when **6** was completely consumed by increasing the reaction time in the presence of *Sel*Fdx1749/*Sel*FdR0978. Collectively, the results suggest that *Sel*Fdx1499 might enable the second round of hydroxylation by inducing some specific conformational changes of PikC to favor the productive binding of **8** and **9**.

Apparently, no common reactivity patterns were observed when the six selected P450s partnered with the same sets of Fdxs/FdRs (Figure 1). The redox partner specificity of a P450 could be either high ($P450_{cam}$) or low (CYP105AS-1). Nonetheless, the phylogenetic analysis of these Fdxs and FdRs provides some important insights into the interactions between these redox partners and P450s. Specifically, the FdRs studied in this work form three major branches in the phylogenetic tree (Figure 1). *Sel*FdR0978, the most efficient FdR, is found to be monophyletic from other FdRs. Multiple protein sequence alignment reveals a common motif ^{197}SLCVRQL^{203} of *Sel*FdR0978, which is the distinguishing feature of the plastidic-type in the family of plant-type FdRs[47] (Figure S1). Four highly conserved motifs mapped in the active site of AdR are found in *Cgl*FdR2658, *Cgl*FdR2719, and *Sco*FdR0681, indicating that they are AdR-like FdRs in the family of GR-type (GR: glutathione reductase) FdRs.[48] The rest of the four FdRs fall into the bacterial-type with the conserved sequence GXG(A)-I(V)XP (Figure S1).[49] Based on the data of catalytic activities (Figure 1), one may deduce that the plastidic-type FdR is more likely to be an efficient FdR in sourcing and transferring electrons for Fdxs.

The phylogenetic analysis of Fdxs shows that the 16 sequences are divided into five branches (Figure 1, Figure S5, Table S1). Branch A has four putative Fe_3S_4 Fdxs and one putative Fe_4S_4 Fdxs that contain only one $Fe_{3/4}S_4$ cluster, among which *Sel*Fdx1749 is predicted to be an Fe_4S_4-type ferredoxin with the cysteine ligands arranged in a $CX_2CX_2CX_nCP$ motif, which is the so-called "classic Fe_4S_4 cluster binding motif",[50] while Fe_3S_4 Fdxs have a similar classic motif except that the second Cys is normally replaced by an Asp.[51] Branch B clusters five predicted Fe_7S_8 Fdxs probably with two iron−sulfur clusters.[52] Identification of a conserved motif of CX_2CGXCX_3CP in subunit II and a second common motif of CX_7C in subunit I provides the evidence for a hybrid Fe_3S_4/Fe_4S_4 cluster in these 7Fe-containing proteins.[18] The remaining six putative Fe_2S_2 Fdxs form three branches: Branch C belongs to the plant-like Fdxs with the conserved motif of $CX_4CX_2CX_{29}C$,[17,53] while Branch D includes two vertebrate-type ferredoxins.[54] *Sel*Fdx0898 is classified as a thioredoxin-like Fdx in that it contains a unique motif of $CX_8CX_{38}CX_3C$ as thioredoxin.[55] Due to the scarcity and sequence uniqueness of thioredoxin-like Fdxs,[56] *Sel*Fdx0898 was not used for establishment of the phylogenetic tree but arbitrarily assigned to Branch E. Interestingly, the majority of positive combinations, especially those showing high and broad spectrum of supporting activities, are well lined with the Fe_2S_2 Fdxs, including *Sel*Fdx0338, *Sel*Fdx1499, and *Cgl*Fdx0526. Notably, Fdxs from the same host organisms could be clustered in distinct branches, suggesting that these genes might have undergone highly divergent evolution or horizontal gene transfers in the long evolutionary history.

Previous studies have shown that Fdxs differ widely in their redox potentials. For example, the midpoint redox potential of Pdx was reported to be −230 mV,[57] spinach Fdx −415 mV,[58] and Adx −270 mV.[59] In this study, the midpoint redox potentials of 16 Fdxs were recorded by protein-film voltammetry with glassy carbon electrode.[60] The E_m value of Pdx was measured to be −243 mV, which is in good agreement with the previous report.[57] The E_m values of 16 Fdxs were determined to be ranging from −216 to −249 mV, with the only exception of *Sel*Fdx0898 being −438 mV (Table S17). However, no correlation between E_m values and Fdx activities was observed. For instance, *Sel*Fdx0898 with the lowest E_m turned out to be an unsatisfactory Fdx (Figure 1). Thus, our results suggest that the redox potential of ferredoxins might not be the key determinant for the P450-supporting activity of an Fdx.

Next, we sought to understand the relationship between the type of Fdx and the productive recognition between an Fdx and a P450 enzyme. It has been well-known that the P450−Fdx recognition is primarily dependent on electrostatic interactions, in particular, the interactions between the negatively charged amino acids on the iron−sulfur side of Fdx and the positively charged residues that are located on the P450 proximal side.[61] Mapping of the electrostatic surfaces of $P450_{cam}$, CreJ, CYP105AS-1, P450sca2, MycG, and PikC revealed that a group of highly conserved Arg and His residues (Figures S6 and S7) form a positively charged rim around a depression that is close to the center of the proximal surface (Figure 3A). These structural features are believed to be crucial for electrostatically steering the transient docking of the negatively charged Fdx, leading to the "encounter complex" to initiate the unidirectional electron transfer from Fdx to P450.[62−64]

Since all the crystal structures of 16 Fdxs have not been solved, we elected to model the structures of these small iron−sulfur proteins using SWISS-MODEL[65] and Phyre2,[66] and all modeled structures were successfully validated by Verify 3D.[67,68] As results, 13 complete Fdx structures were successfully simulated; however, the structures of *Sco*Fdx7110, *Sel*Fdx0698, and *Sel*Fdx1749 were only partially modeled (Figure 3B, Figures S8 and S9). Importantly, there exists a negatively charged surface surrounding the hydrophobic FeS cluster in the Fdxs that shows high and wide-spectrum activities. Detailed structural analysis and molecular simulations of the P450−Fdx complex

DOI: 10.1021/acscatal.8b02913
ACS Catal. 2018, 8, 9992−10003

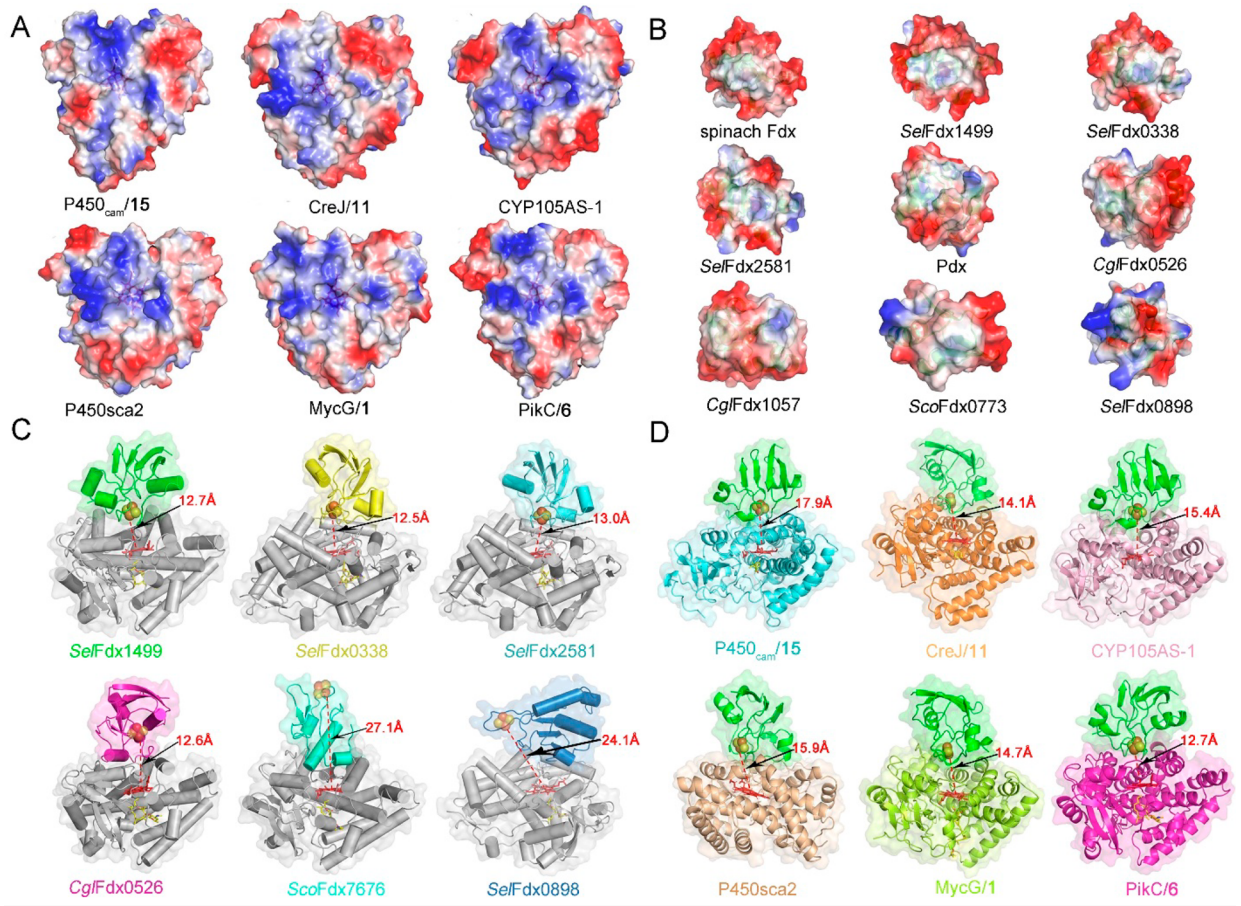

Figure 3. Electrostatic surface analysis and interprotein docking of P450s and Fdxs. (A) Electrostatic surfaces of the six P450 enzymes: $P450_{cam}$/**15** (PDB ID: 2CPP), CreJ/**11** (PDB ID: 5XJN), CYP105AS-1 (substrate-free, PDB ID: 4OQS), P450sca2 (modeled structure with PDB ID: 3CV8 as template), MycG/**1** (PDB ID: 2Y46), and PikC/**6** (PDB ID: 2C6H). (B) Electrostatic surfaces of the representative modeled Fdxs and spinach Fdx (PDB ID: 1A70) and Pdx (PDB ID: 1PDX). (C) The highest scored docking models of the six representative Fdxs in complex with PikC/**6.** The structures of P450-Fdx complexes are shown as cartoon and shaded surface with PikC in gray and Fdxs with different colors (same below). (D) The highest scored docking models of *Sel*Fdx1499 in green in complex with the six individual P450s in different colors. Note: Positively and negatively charged surfaces are colored in blue and red, respectively. Heme and substrates are shown as sticks in red and yellow, respectively. The distances (Å) between the iron−sulfur cluster and heme-iron are indicated by dashed red lines.

structures using ZDOCK Server[69] (ZDOCK 3.0.2) uncovered more structure−function relationships.

First, a compact ($\alpha + \beta$) fold that is typical for Fe_2S_2 ferredoxin[53,54,70] is observed in both plant-type and vertebrate-type Fdxs, as demonstrated by the 3D structures of spinach Fdx[71] and Pdx[33] (Figures S10 and S11), respectively. Electrostatic surface analysis shows that the Fdxs with broad spectra of P450-supporting activities including *Sel*Fdx1499, *Sel*Fdx0338, and *Cgl*Fdx0526 (Figure 1) all have a classic anionic convex surface that is supposed to dock with the basic concave surface of the P450 proximal side.[61,63] Specifically, a highly negatively charged surface is formed around the iron−sulfur cluster loop of *Sel*Fdx1499. By contrast, the corresponding regions of *Sel*Fdx0338 and *Sel*Fdx2581 are found to be moderately and slightly negatively charged, respectively (Figure S8). Thus, this negatively charged extent seems to be roughly consistent with the P450 flexibility of the Branch C Fdxs (Figure 1), again underlining the importance of electrostatic surface potential of Fdxs for P450 recognition. Furthermore, *Sel*Fdx1499, *Sel*Fdx0338, and *Sel*Fdx2581 all contain the conserved motifs of Helix1−3 (Figure S12). A population of conserved acidic amino acids is found on Helix1 and Helix3 of the three plant-like Fdxs. However, the acidic triad of $D_{68}D_{69}D_{70}$ on Helix2 that contributes to the highly negatively charged surface of *Sel*Fdx1499 is replaced by $P_{67}E_{68}P_{69}$ in *Sel*Fdx0338 and $R_{72}R_{75}$ in *Sel*Fdx2581 (Figure S12). The variations of Helix2 could account for their differential binding behaviors with P450s, and hence their reactivity spectra.

Second, although the vertebrate-type (Branch D) and the plant-type (Branch C) Fdxs share the fundamental ($\alpha + \beta$) folding and a similar binding mode of Fe_2S_2 cluster, the location and orientation of Helix2 in Branch D Fdxs differ significantly from those in the plant-type Fdxs.[53,54] Moreover, there exists an additional Helix4 in Branch D Fdxs. Structural simulations and electrostatic surface analysis present some similarities between *Cgl*Fdx0526 and Pdx[33,72] (Figures S8, S9, and S11). The influence of residue variations near the iron−sulfur cluster on the redox potential of Fdxs and hence the rate of electron transfer has been demonstrated by site-directed mutagenesis of other vertebrate-type ferredoxins such as Adx[73−75] and PuxB.[76] Consistently, a number of acidic amino acids on Helix3 that include E65, E66, E68, E69, and D78 (Figure S13) form a strong anionic binding zone in *Cgl*Fdx0526, which might account for its high activity and wide spectrum. By contrast, *Sel*Fdx0698 harbors many positively charged residues on the FeS cluster orientation surface (Figure S8), which may explain

DOI: 10.1021/acscatal.8b02913
ACS Catal. 2018, 8, 9992−10003

its poor activities. The charge distribution of the thioredoxin-like ferredoxin *Sel*Fdx0898 is quite unique. The negatively charged iron−sulfur cluster loop surrounded by a number of basic residues is unlikely to effectively interact with a typical positively charged proximal surface of P450 due to electrostatic repulsions. The sporadic activities of *Sel*Fdx0898 toward the PikC/**6** reactions might be due to a possible special interaction site on the surface of PikC.

Third, it seems difficult to rationalize the reactivity profiles of the Fdxs that belong to Branch A and B solely based on the modeled structures. Nonetheless, *Sco*Fdx0773 and *Sco*Fdx3867 in Branch A, which gave moderate activities in supporting a significant portion of P450 reactions (Figure 1), are found to possess a similar charge distribution pattern on the P450 contacting surface to that of *Cgl*Fdx0526 (Figures S8 and S9).

To further investigate the Fdx−P450 interactions, molecular simulations of the select number of complex structures were performed with ZDOCK analysis.[69,77] As a result (Figure 3C, Figures S14 and S15), the four "good" Fdxs including *Sel*Fdx1499, *Sel*Fdx0338, *Sel*Fdx2581, and *Cgl*Fdx0526 unanimously form a productive "encounter complex" with PikC, in which the distances between the iron−sulfur cluster and heme-iron in the most likely docking modes range from 12.4 to 13.2 Å. Comparatively, other complexes, especially those with the narrowest reactivity spectra, demonstrate significantly longer corresponding distances as exemplified by PikC/*Sco*Fdx7676 (>20 Å, Figure 3C). Two extreme examples are the PikC/*Sco*Fdx7676 and PikC/*Sel*Fdx0898 complexes, in which the Fdx could dock with the distal face rather than the proximal side of the P450 enzyme (Figure S15). These simulation results are consistent with the well-accepted theory that an interprotein electron transfer that is robust and resistant to mutational changes and minor perturbations should have a distance within 14 Å between the electron donor and acceptor.[18] Thus, longer iron−sulfur cluster to heme-iron distances would dramatically decrease the electron transfer rate and hence the catalytic efficiency of the paired P450 enzyme. It is also noteworthy that a majority of Fdxs in Branch A and B can form the complexes through a binding surface other than the FeS cluster loop region (Figures S14 and S15). The formation of these nonproductive "encounter complexes" suggests that the competition between the unfavorable negatively charged surface and the desired iron−sulfur cluster orientation surface during P450 recognition and binding could lead to the slower rate and narrower spectrum of an Fdx of these two classes of ferredoxins.

As one of the superior Fdxs, *Sel*Fdx1499 was modeled to be in complex with each of the six P450 enzymes (Figure 3D). In all cases, the Fe_2S_2 cluster is positioned at a working distance (12−16 Å) via geometric complementation and specific electrostatic interactions, thereby establishing the electron transport pathway. The unsuccessful *Sel*Fdx1499 reactions might be due to its poor docking with FdRs. Notably, these effective Fdx-P450 recognitions can be achieved by different binding modes (Figure 3D). For example, in the PikC/*Sel*Fdx1499 complex, E95 (Helix3 of Fdx) interacts with R62 and H349 (Helix A of PikC); D29, E32, and E33 (Helix1 of Fdx) interact with K105 and R109 (Helix C of PikC) through electrostatic contacts (Figure S16). In the MycG/*Sel*Fdx1499 complex, D69 and D70 (Helix2 of Fdx) electrostatically interact with K100 (Helix C) and R105 (Helix D) of MycG, respectively (Figure S16). These results are in good agreement with the cognition that every interacting interface of an encounter complex might be unique since multiple positively charged residues and the specific contour of a P450 proximal surface would allow it to use a different group of residues to interact with each individual promiscuous redox partner.[78] The highly negatively charged surface of *Sel*Fdx1499 might provide it with more opportunities to form an effective interface with various P450 enzymes. In the case of *Cgl*Fdx0526 (Figure S17), the enriched acidic residues of Helix3 probably make it a very good docking surface toward the proximal face of P450s.

Finally, we practiced the knowledge deduced from this study by predicting the optimal homologous Fdx for PikC. Based on genome searching, there are seven Fdxs encoding genes (Table S1) on the genome of *S. venezuelae* ATCC 15439[79,80] (the host microorganism of PikC), among which the only Fe_2S_2-containing *Svn*Fdx1948 was predicted to be the best ferredoxin for PikC. The molecular docking results (Figure S18) also supported this prediction. Upon heterologous expression in *E. coli* BL21(DE3) and purification of all *Svn*Fdxs, the activities of PikC against **6** were evaluated in vitro using the plastidic-type *Sel*FdR0978 and each individual *Svn*Fdx as redox partners. As predicted, *Svn*Fdx1948 gave the highest substrate conversion of 95% compared to other *Svn*Fdxs; as a control, *Sel*Fdx1499 led to complete substrate conversion (Figure 4).

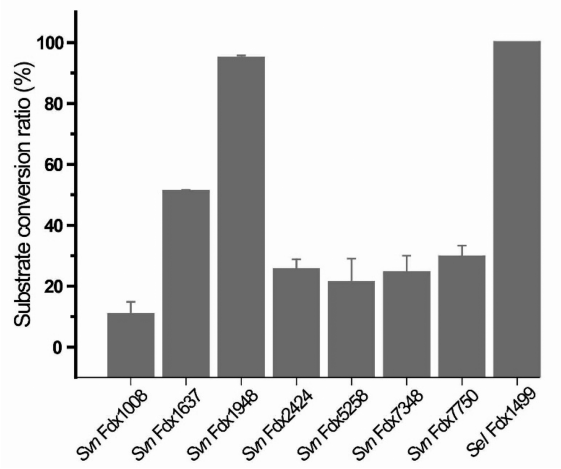

Figure 4. Substrate conversion ratios of the PikC/**6** reactions when partnered with *Sel*FdR0978 and different *Svn*Fdxs from *Streptomyces venezuelae* ATCC 15439. *Sel*Fdx1499 was used as positive control, whose serving reaction's substrate conversion ratio is arbitrarily assigned as 100%.

DISCUSSION

The redox partners mediated electron transfer is often the rate-limiting event in a P450 catalytic cycle.[78,81] FdR, the two-electron carrier, accepts a hydride from NAD(P)H and reduces two equivalents of Fdx in turn. Fdx, the one-electron carrier, directly interacts with P450 and sequentially delivers two electrons for the reductive scission of O_2 by P450. Therefore, a working electron transport pathway requires effective protein−protein interactions of both FdR/Fdx and P450/Fdx, and appropriate potential differences that allow the correct flow direction of electrons.

Despite limited successes in semirational engineering of the P450/Fdx interface,[10,76] rational optimization of the interaction between P450 and Fdx remains challenging due to the lack of intensive understanding of the mechanisms for protein−protein recognition and intermolecular electron transfer.

DOI: 10.1021/acscatal.8b02913
ACS Catal. 2018, 8, 9992−10003

Structural characterization of P450−Fdx complexes has the advantages in addressing this challenge at molecular levels; however, there have been only two available crystal structures of such a complex including the artificial fusion of CYP11A1-Adx[73] and the cross-linked CYP101A1-Pdx.[82]

This study sought to reveal some regular patterns of bacterial P450−redox partner interactions, by which the effective identification of cognate redox partners or optimal surrogate redox partners from multiple Fdx/FdR combinations for the prokaryotic P450 of interest could become possible. Thus, six P450s (seven substrates) that feature high specificity ($P450_{cam}$), functional convergence (CYP105AS-1 and P450sca2), multifunctionality (CreJ and MycG), and substrate flexibility (PikC) were selected. Together with 16 Fdxs and 8 FdRs from three prokaryotic microorganisms, a P450 reaction matrix network consisting of 896 P450 reactions was constituted and comprehensively analyzed.

A proper distance between the FAD of FdR and the iron−sulfur cluster of Fdx is required for the formation of a transient FdR−Fdx complex.[48] The crystal structures of plastidic-type FdRs[83] and GR-type proteins[84,85] revealed that the distance between FAD and the FeS cluster in the plastidic-type complexes is significantly shorter than that in the GR-type complexes (6−8 Å vs 10 Å), suggesting a possible reason for the higher electron transfer efficiency of the former when Fdx binds to the concave surface of FdR. It was also reported that plastidic-type FdRs display higher catalytic turnover rates (200−600 s^{-1}) than the bacterial-type counterparts (2−38 s^{-1}).[86,87] These previous studies might explain the higher efficiency of the plastidic-type *Sel*FdR0978 (Figure 1).

The important finding for Fdx-P450 interactions is that the Fe_2S_2 Fdxs appear to be the specific type of Fdxs favored by different bacterial Class I P450s, according to the reactivity data (Figure 1) and simulation results (Figure 3). This is further supported by the following facts. First, Falkowski and co-workers reported an interesting finding that Fe_2S_2 Fdxs and heme-binding domains might have a single common ancestor,[88] which suggests functional connections and coevolution of these two protein families. Second, the most efficient native Fdx for PikC was proven to be the only Fe_2S_2 Fdx *Svn*Fdx1948 based on in vitro experiments (Figure 4). Third, FdxH, one of the Fe_2S_2-containing Fdxs from *S. avermitilis* MA4680, was recently identified as the optimal endogenous redox partner for CYP105D7 based on in vitro activity reconstitution, gene disruption, and mRNA expression profile analysis.[89] Fourth, the most popular surrogate ferredoxins including spinach Fdx, Pdx, and Adx all belong to the Fe_2S_2 type. However, many *Streptomyces* spp. only possess non-Fe_2S_2 Fdxs[13,90] due to some unknown evolutionary reasons. Thus, we hypothesize that the in vivo activity of a *Streptomyces* P450 enzyme could be improved by introduction of a gene that encodes a more efficient Fe_2S_2 type Fdx into the bacterial genome. More experiments are required for testing this industrially important hypothesis, which are currently ongoing in our laboratory.

Mechanistically, the Fe_2S_2 cluster can be placed at an appropriate position for effective electron transfer through geometric complementation and the electrostatically steered interactions (Figure 3, Figures S14 and S15). The convex hydrophobic iron−sulfur cluster loop of an Fdx also plays an important role in expelling the water molecules residing around the concave of proximal surface of the P450, thus driving the P450−Fdx binding entropically.[18] Interestingly, all four "good" Fdxs including *Sel*Fdx1499, *Sel*Fdx0338, *Sel*Fdx2581, and *Cgl*Fdx0526 seem to follow this binding logic (Figure 3B). However, some special interactions within the encounter complex must also be taken into account due to the molecular diversity of Fdxs and P450s, which indeed complicates the explanation and the prediction of the supporting activity of an Fdx toward a specific P450 enzyme. In the well-studied $P450_{cam}$/Pdx/**15** system, the binding of Pdx results in P450 structural changes that are required for catalytic activity.[91,92] In the meantime, the conformational changes of P450 induced by substrate binding may also influence the docking mode of Pdx.[93] In this study, PikC/**6** and PikC/**7** showed distinct reactivity patterns against the identical suites of Fdxs/FdRs, which reinforces the mutual impacts among P450, substrate, Fdx, and FdR.

Taken together, we suggest that a certain bacterial P450 enzyme might have evolved to favor a specific combination of Fdx and FdR among multiple redox partner proteins toward a specific functionality, although some other redox partners could be functionally complementary.[94,95] In other words, the selectivity and redundancy of Fdxs in a microorganism likely coexist. This could be physiologically important since the expression levels and catalytic activities of redox partners need to be continuously tuned without losing the balance between specificity, affinity, and efficiency in order to adapt to different developmental stages and ever-changing environments. By contrast, a small number of P450 enzymes such as $P450_{cam}$[34] and $P450_{SU1}$[96] show very high selectivity toward Fdx, likely due to their highly specialized functions. The naturally P450−redox partner fusion proteins represent an extreme with the fixed selectivity.[97,98]

It has widely been accepted that the optimal redox partners for a P450 enzyme should be homogeneous ones, especially the cotranscribed redox partners, due to possible coevolution.[99] However, this postulate has not been tested experimentally. In the reaction matrix network (Figure 1), the cognate and cotranscribed redox partners *Cgl*FdR0525/*Cgl*Fdx0526[35] only represented one of the five best CreJ companions, suggesting that the endogenous electron transfer chain may not necessarily be the best choice for a specific CYP. Heterologous redox partners could also form an efficient hybrid electron transport pathway. This finding could be important for optimization of the biosynthetic pathways that involve P450-catalyzed step(s) in industrial strain improvement.

Recently, we reported an exceptional finding that the use of the surrogate redox partner RhFRED not only altered the catalytic efficiency and product distribution of MycG but also led to the change of the type and site-selectivity of MycG reactions, giving rise to a number of unnatural *N*-demethylation products.[28] An open question is whether this phenomenon has generality. In this study, no similar demethylation products were observed in the tested MycG reactions. Although novel products **22** and **24** were observed in CYP105AS-1/**18** and PikC/**6** reactions (Figure 2), respectively, they are virtually overoxidation products, and the reaction type and selectivity did not change. Therefore, the unique behavior of MycG/RhFRED seems not to be general at least based on the current evidence. It also suggests that, unlike Fdxs, RhFRED might interact with a P450 enzyme via an alternative interface.

In conclusion, the efficiency of the electron transport pathway in a bacterial Class I P450 system is determined by mutual interactions of five elements including P450, Fdx, FdR, substrate, and NAD(P)H. The substrate binding initiates the P450 catalytic cycle and induces structural changes of P450

DOI: 10.1021/acscatal.8b02913
ACS Catal. 2018, 8, 9992−10003

including the conformational changes of the Fdx docking interface that is located on the proximal side, which in turn affects the P450's preference toward Fdx via electrostatic interactions and steric complementation. Similar interactions between Fdx and FdR, and the efficiency of FdR in sourcing electrons from NAD(P)H, could also influence the overall electron transfer rates and the catalytic efficiency. In addition to the key productive protein−protein interactions, appropriate redox potential differences among P450, Fdx, and FdR are also important factors to be considered.

Based on our results, there seem to be no strict rules to guide the selection of redox partners for a specific P450 reaction. For an important P450 reaction, we suggest that the best way to determine the optimal redox partners might be the activity screening using various Fdx/FdR combinations before the transient protein−protein interactions and the redox potentials of all components could be accurately calculated and evaluated. Nonetheless, Fdx-P450 molecular docking could provide useful information for predicting workable Fdxs for a specific P450 enzyme, especially when the crystal structure of the P450 enzyme is available. Finally, several empirical rules could be proposed for further examinations: (1) the plastidic-type FdR and the Fe_2S_2 Fdx are more likely to provide high electron transfer efficiency for a bacterial Class I P450 enzyme; (2) the native redox partners are not necessarily the optimal choices for a P450 of interest; (3) it is not necessarily better to use the most efficient redox partner for a specific P450 reaction since the undesired overoxidation could occur; and (4) redox partners could be utilized to generate more oxidative derivatives.

■ ASSOCIATED CONTENT

Supporting Information

The Supporting Information is available free of charge on the ACS Publications website at DOI: 10.1021/acscatal.8b02913.

Experimental methods, vectors preparation, protein expression and purification, and electrochemical redox potential measurements, structural simulation, molecular docking, NMR data, etc. (PDF)

■ AUTHOR INFORMATION

Corresponding Author

*E-mail: lishengying@qibebt.ac.cn.

ORCID

Wei Zhang: 0000-0001-9459-680X

Lei Han: 0000-0003-1955-0718

Shengying Li: 0000-0002-5244-870X

Author Contributions

†These authors (W.Z. and L.D.) contributed equally to this work.

Notes

The authors declare no competing financial interest.

■ ACKNOWLEDGMENTS

We are grateful to Dr. Huifang Xu at Qingdao Institute of Bioenergy and Bioprocess Technology, Chinese Academy of Sciences, for proofreading the manuscript and helpful discussion. This work was supported by the Shandong Provincial Natural Science Foundation (ZR2017ZB0207 to W.Z. and S.L., and ZR2016CB10 to F.Q.), the National Natural Science Foundation of China (grants 81741155, 31422002, and 21472204 to S.L., 31570030 to W.Z.), the Qilu Youth Scholar Startup Funding of Shandong University (to W.Z.), Chinese Academy of Sciences (grants QYZDB-SSW-SMC042 to S.L.), the National Postdoctoral Innovative Talent Support Program (BX20180325 to L.D.), and China Postdoctoral Science Foundation (188229 to F.L.).

■ REFERENCES

(1) Coon, M. J. Nature's Most Versatile Biological Catalyst. *Annu. Rev. Pharmacol. Toxicol.* **2005**, *45*, 1−25.

(2) Montellano, P. R. O. d. *Cytochrome P450: Structure, mechanism, and biochemistry*, 3rd ed.; Kluwer Academic/Plenum: New York, 2005.

(3) O'Reilly, E.; Kohler, V.; Flitsch, S. L.; Turner, N. J. Cytochromes P450 as Useful Biocatalysts: Addressing the Limitations. *Chem. Commun. (Cambridge, U. K.)* **2011**, *47*, 2490−2501.

(4) Munro, A. W.; Girvan, H. M.; Mason, A. E.; Dunford, A. J.; McLean, K. J. What Makes a P450 Tick? *Trends Biochem. Sci.* **2013**, *38*, 140−150.

(5) Girvan, H. M.; Munro, A. W. Applications of Microbial Cytochrome P450 Enzymes in Biotechnology and Synthetic Biology. *Curr. Opin. Chem. Biol.* **2016**, *31*, 136−145.

(6) Zhang, X.; Li, S. Expansion of Chemical Space for Natural Products by Uncommon P450 Reactions. *Nat. Prod. Rep.* **2017**, *34*, 1061−1089.

(7) McLean, K. J.; Luciakova, D.; Belcher, J.; Tee, K. L.; Munro, A. W. Biological Diversity of Cytochrome P450 Redox Partner Systems. *Adv. Exp. Med. Biol.* **2015**, *851*, 299−317.

(8) Li, S. Y.; Podust, L. M.; Sherman, D. H. Engineering and Analysis of a Self-sufficient Biosynthetic Cytochrome P450 PikC Fused to the RhFRED Reductase Domain. *J. Am. Chem. Soc.* **2007**, *129*, 12940−12941.

(9) Robin, A.; Kohler, V.; Jones, A.; Ali, A.; Kelly, P. P.; O'Reilly, E.; Turner, N. J.; Flitsch, S. L. Chimeric Self-sufficient $P450_{cam}$-RhFRed Biocatalysts with Broad Substrate Scope. *Beilstein J. Org. Chem.* **2011**, *7*, 1494−1498.

(10) Ba, L.; Li, P.; Zhang, H.; Duan, Y.; Lin, Z. L. Semi-Rational Engineering of Cytochrome P450sca-2 in a Hybrid System for Enhanced Catalytic Activity: Insights into the Important Role of Electron Transfer. *Biotechnol. Bioeng.* **2013**, *110*, 2815−2825.

(11) Tosha, T.; Yoshioka, S.; Hori, H.; Takahashi, S.; Ishimori, K.; Morishima, I. Molecular Mechanism of the Electron Transfer Reaction in Cytochrome P450(cam)–Putidaredoxin: Roles of Glutamine 360 at the Heme Proximal Site. *Biochemistry* **2002**, *41*, 13883−13893.

(12) Lamb, D. C.; Waterman, M. R. Unusual Properties of the Cytochrome P450 Superfamily. *Philos. Trans. R. Soc., B* **2013**, *368*, 20120434.

(13) Chun, Y. J.; Shimada, T.; Sanchez-Ponce, R.; Martin, M. V.; Lei, L.; Zhao, B.; Kelly, S. L.; Waterman, M. R.; Lamb, D. C.; Guengerich, F. P. Electron Transport Pathway for a *Streptomyces* Cytochrome P450: Cytochrome P450 105D5-catalyzed Fatty Acid Hydroxylation in *Streptomyces coelicolor* A3(2). *J. Biol. Chem.* **2007**, *282*, 17486−17500.

(14) Kalinowski, J.; Bathe, B.; Bartels, D.; Bischoff, N.; Bott, M.; Burkovski, A.; Dusch, N.; Eggeling, L.; Eikmanns, B. J.; Gaigalat, L.; Goesmann, A.; Hartmann, M.; Huthmacher, K.; Kramer, R.; Linke, B.; McHardy, A. C.; Meyer, F.; Mockel, B.; Pfefferle, W.; Puhler, A.; Rey, D. A.; Ruckert, C.; Rupp, O.; Sahm, H.; Wendisch, V. F.; Wiegrabe, I.; Tauch, A. The Complete *Corynebacterium glutamicum* ATCC 13032 Genome Sequence and Its Impact on the Production of L-aspartate-derived Amino Acids and Vitamins. *J. Biotechnol.* **2003**, *104*, 5−25.

(15) Stork, T.; Laxa, M.; Dietz, M. S.; Dietz, K. J. Functional Characterisation of the Peroxiredoxin Gene Family Members of *Synechococcus elongatus* PCC 7942. *Arch. Microbiol.* **2009**, *191*, 141−151.

DOI: 10.1021/acscatal.8b02913
ACS Catal. 2018, 8, 9992−10003

(16) Brzoska, K.; Meczynska, S.; Kruszewski, M. Iron−Sulfur Cluster Proteins: Electron Transfer and Beyond. *Acta Biochim. Polym.* **2006**, *53*, 685−691.
(17) Meyer, J. Iron-sulfur Protein Folds, Iron-sulfur Chemistry, and Evolution. *JBIC, J. Biol. Inorg. Chem.* **2008**, *13*, 157−170.
(18) Liu, J.; Chakraborty, S.; Hosseinzadeh, P.; Yu, Y.; Tian, S.; Petrik, I.; Bhagi, A.; Lu, Y. Metalloproteins Containing Cytochrome, Iron-sulfur, or Copper Redox Centers. *Chem. Rev.* **2014**, *114*, 4366−4469.
(19) Koga, H.; Yamaguchi, E.; Matsunaga, K.; Aramaki, H.; Horiuchi, T. Cloning and Nucleotide Aequences of NADH-putidaredoxin Reductase Gene (camA) and Putidaredoxin Gene (camB) Involved in Cytochrome P-450$_{cam}$ Hydroxylase of *Pseudomonas putida*. *J. Biochem.* **1989**, *106*, 831−836.
(20) Fang, B.; Xu, H.; Liu, Y.; Qi, F.; Zhang, W.; Chen, H.; Wang, C.; Wang, Y.; Yang, W.; Li, S. Mutagenesis and Redox Partners Analysis of the P450 Fatty Acid Decarboxylase OleT$_{JE}$. *Sci. Rep.* **2017**, *7*, 44258−44264.
(21) Kern, F.; Dier, T. K. F.; Khatri, Y.; Ewen, K. M.; Jacquot, J. P.; Volmer, D. A.; Bernhardt, R. Highly Efficient CYP167A1 (EpoK) Dependent Epothilone B Formation and Production of 7-Ketone Epothilone D as a New Epothilone Derivative. *Sci. Rep.* **2015**, *5*, 14881−14893.
(22) Li, M.; Guo, W.; Chen, X. A Novel NADPH-dependent Reductase of *Sulfobacillus acidophilus* TPY Phenol Hydroxylase: Expression, Characterization, and Functional Analysis. *Appl. Microbiol. Biotechnol.* **2016**, *100*, 10417−10428.
(23) Bell, S. G.; Dale, A.; Rees, N. H.; Wong, L. L. A Cytochrome P450 Class I Electron Transfer System from *Novosphingobium aromaticivorans*. *Appl. Microbiol. Biotechnol.* **2010**, *86*, 163−175.
(24) Girhard, M.; Klaus, T.; Khatri, Y.; Bernhardt, R.; Urlacher, V. B. Characterization of the Versatile Monooxygenase CYP109B1 from *Bacillus subtilis*. *Appl. Microbiol. Biotechnol.* **2010**, *87*, 595−607.
(25) Anzai, Y.; Li, S.; Chaulagain, M. R.; Kinoshita, K.; Kato, F.; Montgomery, J.; Sherman, D. H. Functional Analysis of MycCI and MycG, Cytochrome P450 Enzymes Involved in Biosynthesis of Mycinamicin Macrolide Antibiotics. *Chem. Biol.* **2008**, *15*, 950−959.
(26) Anzai, Y.; Saito, N.; Tanaka, M.; Kinoshita, K.; Koyama, Y.; Kato, F. Organization of the Biosynthetic Gene Cluster for the Polyketide Macrolide Mycinamicin in *Micromonospora griseorubida*. *FEMS Microbiol. Lett.* **2003**, *218*, 135−141.
(27) Inouye, M.; Takada, Y.; Muto, N.; Beppu, T.; Horinouchi, S. Characterization and Expression of a P-450-like Mycinamicin Biosynthesis Gene using a Novel *Micromonospora-Escherichia coli* Shuttle Cosmid Vector. *Mol. Gen. Genet.* **1994**, *245*, 456−464.
(28) Zhang, W.; Liu, Y.; Yan, J.; Cao, S.; Bai, F.; Yang, Y.; Huang, S.; Yao, L.; Anzai, Y.; Kato, F.; Podust, L. M.; Sherman, D. H.; Li, S. New Reactions and Products Resulting from Alternative Interactions between the P450 Enzyme and Redox Partners. *J. Am. Chem. Soc.* **2014**, *136*, 3640−3646.
(29) Li, S.; Chaulagain, M. R.; Knauff, A. R.; Podust, L. M.; Montgomery, J.; Sherman, D. H. Selective Oxidation of Carbolide C-H Bonds by an Engineered Macrolide P450 Monooxygenase. *Proc. Natl. Acad. Sci. U. S. A.* **2009**, *106*, 18463−18468.
(30) Sibbesen, O.; De Voss, J. J.; de Montellano, P. R. Putidaredoxin Reductase-Putidaredoxin-Cytochrome P450cam Triple Fusion Protein. Construction of a Self-sufficient *Escherichia coli* Catalytic System. *J. Biol. Chem.* **1996**, *271*, 22462−22469.
(31) Auclair, K.; Moenne-Loccoz, P.; Ortiz de Montellano, P. R. Roles of the Proximal Heme Thiolate Ligand in Cytochrome P450(cam). *J. Am. Chem. Soc.* **2001**, *123*, 4877−4885.
(32) McLean, K. J.; Hans, M.; Meijrink, B.; van Scheppingen, W. B.; Vollebregt, A.; Tee, K. L.; van der Laan, J. M.; Leys, D.; Munro, A. W.; van den Berg, M. A. Single-step Fermentative Production of the Cholesterol-lowering Drug Pravastatin via Reprogramming of *Penicillium chrysogenum*. *Proc. Natl. Acad. Sci. U. S. A.* **2015**, *112*, 2847−2852.
(33) Sevrioukova, I. F.; Garcia, C.; Li, H.; Bhaskar, B.; Poulos, T. L. Crystal Structure of Putidaredoxin, the [2Fe-2S] Component of the P450$_{cam}$ Monooxygenase System from *Pseudomonas putida*. *J. Mol. Biol.* **2003**, *333*, 377−392.
(34) Sevrioukova, I. F.; Poulos, T. L. Structural Biology of Redox Partner Interactions in P450cam Monooxygenase: a Fresh Look at an Old System. *Arch. Biochem. Biophys.* **2011**, *507*, 66−74.
(35) Du, L.; Dong, S.; Zhang, X. W.; Jiang, C. Y.; Chen, J. F.; Yao, L. S.; Wang, X.; Wan, X. B.; Liu, X.; Wang, X. Q.; Huang, S. H.; Cui, Q.; Feng, Y. G.; Liu, S. J.; Li, S. Y. Selective Oxidation of Aliphatic C-H Bonds in Alkylphenols by a Chemomimetic Biocatalytic System. *Proc. Natl. Acad. Sci. U. S. A.* **2017**, *114*, E5129−E5137.
(36) Du, L.; Ma, L.; Qi, F.; Zheng, X.; Jiang, C.; Li, A.; Wan, X.; Liu, S. J.; Li, S. Characterization of a Unique Pathway for 4-Cresol Catabolism Initiated by Phosphorylation in *Corynebacterium glutamicum*. *J. Biol. Chem.* **2016**, *291*, 6583−6594.
(37) Li, T.; Chen, X.; Chaudhry, M. T.; Zhang, B.; Jiang, C. Y.; Liu, S. J. Genetic Characterization of 4-Cresol Catabolism in *Corynebacterium glutamicum*. *J. Biotechnol.* **2014**, *192*, 355−365.
(38) Lamon-Fava, S. Statins and Lipid Metabolism: an Update. *Curr. Opin. Lipidol.* **2013**, *24*, 221−226.
(39) Lewis, D. F. V.; Hlavica, P. Interactions between Redox Partners in Various Cytochrome P450 Systems: Functional and Structural Aspects. *Biochim. Biophys. Acta, Bioenerg.* **2000**, *1460*, 353−374.
(40) Everett, D. W.; Chando, T. J.; Didonato, G. C.; Singhvi, S. M.; Pan, H. Y.; Weinstein, S. H. Biotransformation of Pravastatin Sodium in Humans. *Drug Metab. Dispos.* **1991**, *19*, 740−748.
(41) Muramatsu, S.; Komokata, Y.; Tanaka, Y.; Takahagi, H. Metabolism of Pravastatin Sodium by 3 Alpha-hydroxysteroid Dehydrogenase. *Biol. Pharm. Bull.* **1997**, *20*, 1199−1203.
(42) Xue, Y. Q.; Wilson, D.; Zhao, L. S.; Liu, H. W.; Sherman, D. H. Hydroxylation of Macrolactones YC-17 and Narbomycin is Mediated by the PikC-encoded Cytochrome P450 in *Streptomyces venezuelae*. *Chem. Biol.* **1998**, *5*, 661−667.
(43) Negretti, S.; Narayan, A. R.; Chiou, K. C.; Kells, P. M.; Stachowski, J. L.; Hansen, D. A.; Podust, L. M.; Montgomery, J.; Sherman, D. H. Directing Group-controlled Regioselectivity in an Enzymatic C-H Bond Oxygenation. *J. Am. Chem. Soc.* **2014**, *136*, 4901−4904.
(44) Miles, C. S.; Ost, T. W.; Noble, M. A.; Munro, A. W.; Chapman, S. K. Protein Engineering of Cytochromes P-450. *Biochim. Biophys. Acta, Protein Struct. Mol. Enzymol.* **2000**, *1543*, 383−407.
(45) Zhang, Q.; Sherman, D. H. Isolation and Structure Determination of Novamethymycin, a New Bioactive Metabolite of the Methymycin Biosynthetic Pathway in *Streptomyces venezuelae*. *J. Nat. Prod.* **2001**, *64*, 1447−1450.
(46) Hansen, D. A.; Rath, C. M.; Eisman, E. B.; Narayan, A. R. H.; Kittendorf, J. D.; Mortison, J. D.; Yoon, Y. J.; Sherman, D. H. Biocatalytic Synthesis of Pikromycin, Methymycin, Neomethymycin, Novamethymycin, and Ketomethymycin. *J. Am. Chem. Soc.* **2013**, *135*, 11232−11238.
(47) Nascimento, A. S.; Catalano-Dupuy, D. L.; Bernardes, A.; Neto, M.; Santos, M. A.; Ceccarelli, E. A.; Polikarpov, I. Crystal Structures of *Leptospira interrogans* FAD-containing Ferredoxin-NADP$^+$ Reductase and Its Complex with NADP$^+$. *BMC Struct. Biol.* **2007**, *7*, 69−80.
(48) Aliverti, A.; Pandini, V.; Pennati, A.; de Rosa, M.; Zanetti, G. Structural and Functional Diversity of Ferredoxin-NADP$^+$ Reductases. *Arch. Biochem. Biophys.* **2008**, *474*, 283−291.
(49) Ingelman, M.; Bianchi, V.; Eklund, H. The Three-dimensional Structure of Flavodoxin Reductase from *Escherichia coli* at 1.7 Å Resolution. *J. Mol. Biol.* **1997**, *268*, 147−157.
(50) Cammack, R. Iron-Sulfur Clusters in Enzymes - Themes and Variations. *Adv. Inorg. Chem.* **1992**, *38*, 281−322.
(51) Hannan, J. P.; Busch, J. L.; Breton, J.; James, R.; Thomson, A. J.; Moore, G. R.; Davy, S. L. Characterisation of Oxidised 7Fe Dicluster Ferredoxins with NMR Spectroscopy. *JBIC, J. Biol. Inorg. Chem.* **2000**, *5*, 432−447.
(52) Otaka, E.; Ooi, T. Examination of Protein Sequence Homologies: IV. Twenty-seven Bacterial Ferredoxins. *J. Mol. Evol.* **1987**, *26*, 257−267.

DOI: 10.1021/acscatal.8b02913
ACS Catal. 2018, 8, 9992−10003

(53) Fukuyama, K. Structure and Function of Plant-type Ferredoxins. *Photosynth. Res.* **2004**, *81*, 289−301.
(54) Muller, J. J.; Muller, A.; Rottmann, M.; Bernhardt, R.; Heinemann, U. Vertebrate-type and Plant-type Ferredoxins: Crystal Structure Comparison and Electron Transfer Pathway Modelling. *J. Mol. Biol.* **1999**, *294*, 501−513.
(55) Yeh, A. P.; Chatelet, C.; Soltis, S. M.; Kuhn, P.; Meyer, J.; Rees, D. C. Structure of a Thioredoxin-like [2Fe-2S] Ferredoxin from *Aquifex aeolicus*. *J. Mol. Biol.* **2000**, *300*, 587−595.
(56) Meyer, J. Ferredoxins of the Third Kind. *FEBS Lett.* **2001**, *509*, 1−5.
(57) Stephens, P. J.; Jollie, D. R.; Warshel, A. Protein Control of Redox Potentials of Iron-sulfur Proteins. *Chem. Rev.* **1996**, *96*, 2491−2513.
(58) Cammack, R.; Rao, K. K.; Bargeron, C. P.; Hutson, K. G.; Andrew, P. W.; Rogers, L. J. Midpoint Redox Potentials of Plant and Algal Ferredoxins. *Biochem. J.* **1977**, *168*, 205−209.
(59) Uhlmann, H.; Iametti, S.; Vecchio, G.; Bonomi, F.; Bernhardt, R. Pro108 is Important for Folding and Stabilization of Adrenal Ferredoxin, but does not Influence the Functional Properties of the Protein. *Eur. J. Biochem.* **1997**, *248*, 897−902.
(60) Fleming, B. D.; Tian, Y.; Bell, S. G.; Wong, L. L.; Urlacher, V.; Hill, H. A. Redox Properties of Cytochrome P450BM3 Measured by Direct Methods. *Eur. J. Biochem.* **2003**, *270*, 4082−4088.
(61) Wada, A.; Waterman, M. R. Identification by Site-Directed Mutagenesis of Two Lysine Residues in Cholesterol Side Chain Cleavage Cytochrome P450 That Are Essential for Adrenodoxin Binding. *J. Biol. Chem.* **1992**, *267*, 22877−22882.
(62) Schilder, J.; Ubbink, M. Formation of Transient Protein Complexes. *Curr. Opin. Struct. Biol.* **2013**, *23*, 911−918.
(63) Hlavica, P.; Schulze, J.; Lewis, D. F. Functional Interaction of Cytochrome P450 with Its Redox Partners: a Critical Assessment and Update of the Topology of Predicted Contact Regions. *J. Inorg. Biochem.* **2003**, *96*, 279−297.
(64) Page, C. C.; Moser, C. C.; Dutton, P. L. Mechanism for Electron Transfer within and between Proteins. *Curr. Opin. Chem. Biol.* **2003**, *7*, 551−556.
(65) Biasini, M.; Bienert, S.; Waterhouse, A.; Arnold, K.; Studer, G.; Schmidt, T.; Kiefer, F.; Gallo Cassarino, T.; Bertoni, M.; Bordoli, L.; Schwede, T. SWISS-MODEL: Modelling Protein Tertiary and Quaternary Structure Using Evolutionary Information. *Nucleic Acids Res.* **2014**, *42*, W252−W258.
(66) Kelley, L. A.; Mezulis, S.; Yates, C. M.; Wass, M. N.; Sternberg, M. J. The Phyre2 Web Portal for Protein Modeling, Prediction and Analysis. *Nat. Protoc.* **2015**, *10*, 845−858.
(67) Bowie, J. U.; Luthy, R.; Eisenberg, D. A Method to Identify Protein Sequences that Fold into a Known Three-dimensional Structure. *Science* **1991**, *253*, 164−170.
(68) Luthy, R.; Bowie, J. U.; Eisenberg, D. Assessment of Protein Models with Three-dimensional Profiles. *Nature* **1992**, *356*, 83−85.
(69) Pierce, B. G.; Wiehe, K.; Hwang, H.; Kim, B. H.; Vreven, T.; Weng, Z. ZDOCK Server: Interactive Docking Prediction of Protein-protein Complexes and Symmetric Multimers. *Bioinformatics* **2014**, *30*, 1771−1773.
(70) Krishna, S. S.; Sadreyev, R. I.; Grishin, N. V. A Tale of Two Ferredoxins: Sequence Similarity and Structural Differences. *BMC Struct. Biol.* **2006**, *6*, 8−14.
(71) Binda, C.; Coda, A.; Aliverti, A.; Zanetti, G.; Mattevi, A. Structure of the Mutant E92K of [2Fe-2S] Ferredoxin I from *Spinacia oleracea* at 1.7 Å Resolution. *Acta Crystallogr., Sect. D: Biol. Crystallogr.* **1998**, *54*, 1353−1358.
(72) Muller, A.; Muller, J. J.; Muller, Y. A.; Uhlmann, H.; Bernhardt, R.; Heinemann, U. New Aspects of Electron Transfer Revealed by the Crystal Structure of a Truncated Bovine Adrenodoxin, Adx(4−108). *Structure* **1998**, *6*, 269−280.
(73) Strushkevich, N.; MacKenzie, F.; Cherkesova, T.; Grabovec, I.; Usanov, S.; Park, H. W. Structural Basis for Pregnenolone Biosynthesis by the Mitochondrial Monooxygenase System. *Proc. Natl. Acad. Sci. U. S. A.* **2011**, *108*, 10139−10143.
(74) Ewen, K. M.; Ringle, M.; Bernhardt, R. Adrenodoxin–a Versatile Ferredoxin. *IUBMB Life* **2012**, *64*, 506−512.
(75) Ewen, K. M.; Kleser, M.; Bernhardt, R. Adrenodoxin: the Archetype of Vertebrate-type [2Fe-2S] Cluster Ferredoxins. *Biochim. Biophys. Acta, Proteins Proteomics* **2011**, *1814*, 111−125.
(76) Bell, S. G.; McMillan, J. H. C.; Yorke, J. A.; Kavanagh, E.; Johnson, E. O. D.; Wong, L. L. Tailoring an Alien Ferredoxin to Support Native-like P450 Monooxygenase Activity. *Chem. Commun. (Cambridge, U. K.)* **2012**, *48*, 11692−11694.
(77) Pierce, B. G.; Hourai, Y.; Weng, Z. Accelerating Protein Docking in ZDOCK Using an Advanced 3D Convolution Library. *PLoS One* **2011**, *6*, No. e24657.
(78) Waskell, L.; Kim, J.-J. P. Electron Transfer Partners of Cytochrome P450. In *Cytochrome P450: Structure, Mechanism, and Biochemistry*, 4th ed.; Ortiz de Montellano, P. R., Ed.; Springer International Publishing: Cham, 2015; Vol. *1*, pp 33−68.
(79) He, J.; Sundararajan, A.; Devitt, N. P.; Schilkey, F. D.; Ramaraj, T.; Melancon, C. E., III. Complete Genome Sequence of *Streptomyces venezuelae* ATCC 15439, Producer of the Methymycin/Pikromycin Family of Macrolide Antibiotics, Using PacBio Technology. *Genome Announc.* **2016**, *4*, e00337-16.
(80) Song, J. Y.; Yoo, Y. J.; Lim, S. K.; Cha, S. H.; Kim, J. E.; Roe, J. H.; Kim, J. F.; Yoon, Y. J. Complete Genome Sequence of *Streptomyces venezuelae* ATCC 15439, a Promising Cell Factory for Production of Secondary Metabolites. *J. Biotechnol.* **2016**, *219*, 57−58.
(81) Hlavica, P., Mechanistic Basis of Electron Transfer to Cytochromes P450 by Natural Redox Partners and Artificial Donor Constructs. In *Monooxygenase, Peroxidase and Peroxygenase Properties and Mechanisms of Cytochrome P450*; Hrycay, E. G., Bandiera, S. M., Eds.; Springer: Cham, 2015; Vol. *851*, pp 247−297.
(82) Tripathi, S.; Li, H.; Poulos, T. L. Structural Basis for Effector Control and Redox Partner Recognition in Cytochrome P450. *Science* **2013**, *340*, 1227−1230.
(83) Kurisu, G.; Kusunoki, M.; Katoh, E.; Yamazaki, T.; Teshima, K.; Onda, Y.; Kimata-Ariga, Y.; Hase, T. Structure of the Electron Transfer Complex between Ferredoxin and Ferredoxin-NADP$^+$ Reductase. *Nat. Struct. Biol.* **2001**, *8*, 117−121.
(84) Hagelueken, G.; Wiehlmann, L.; Adams, T. M.; Kolmar, H.; Heinz, D. W.; Tummler, B.; Schubert, W. D. Crystal Structure of the Electron Transfer Complex Rubredoxin-rubredoxin Reductase of *Pseudomonas aeruginosa*. *Proc. Natl. Acad. Sci. U. S. A.* **2007**, *104*, 12276−12281.
(85) Muller, J. J.; Lapko, A.; Bourenkov, G.; Ruckpaul, K.; Heinemann, U. Adrenodoxin Reductase-adrenodoxin Complex Structure Suggests Electron Transfer Path in Steroid Biosynthesis. *J. Biol. Chem.* **2001**, *276*, 2786−2789.
(86) Musumeci, M. A.; Botti, H.; Buschiazzo, A.; Ceccarelli, E. A. Swapping FAD Binding Motifs between Plastidic and Bacterial Ferredoxin-NADP(H) Reductases. *Biochemistry* **2011**, *50*, 2111−2122.
(87) Ceccarelli, E. A.; Arakaki, A. K.; Cortez, N.; Carrillo, N. Functional Plasticity and Catalytic Efficiency in Plant and Bacterial Ferredoxin-NADP(H) Reductases. *Biochim. Biophys. Acta, Proteins Proteomics* **2004**, *1698*, 155−165.
(88) Harel, A.; Bromberg, Y.; Falkowski, P. G.; Bhattacharya, D. Evolutionary History of Redox Metal-binding Domains across the Tree of Life. *Proc. Natl. Acad. Sci. U. S. A.* **2014**, *111*, 7042−7047.
(89) Pandey, B. P.; Lee, N.; Choi, K. Y.; Kim, J. N.; Kim, E. J.; Kim, B. G. Identification of the Specific Electron Transfer Proteins, Ferredoxin, and Ferredoxin Reductase, for CYP105D7 in *Streptomyces avermitilis* MA4680. *Appl. Microbiol. Biotechnol.* **2014**, *98*, 5009−5017.
(90) Lamb, D. C.; Skaug, T.; Song, H. L.; Jackson, C. J.; Podust, L. M.; Waterman, M. R.; Kell, D. B.; Kelly, D. E.; Kelly, S. L. The Cytochrome P450 Complement (CYPome) of *Streptomyces coelicolor* A3(2). *J. Biol. Chem.* **2002**, *277*, 24000−24005.
(91) Poulos, T. L. Heme Enzyme Structure and Function. *Chem. Rev.* **2014**, *114*, 3919−3962.

DOI: 10.1021/acscatal.8b02913
ACS Catal. 2018, 8, 9992−10003

(92) Hollingsworth, S. A.; Batabyal, D.; Nguyen, B. D.; Poulos, T. L. Conformational Selectivity in Cytochrome P450 Redox Partner Interactions. *Proc. Natl. Acad. Sci. U. S. A.* **2016**, *113*, 8723−8728.
(93) Batabyal, D.; Richards, L. S.; Poulos, T. L. Effect of Redox Partner Binding on Cytochrome P450 Conformational Dynamics. *J. Am. Chem. Soc.* **2017**, *139*, 13193−13199.
(94) Hannemann, F.; Bichet, A.; Ewen, K. M.; Bernhardt, R. Cytochrome P450 Systems - Biological Variations of Electron Transport Chains. *Biochim. Biophys. Acta, Gen. Subj.* **2007**, *1770*, 330−344.
(95) McLean, K. J.; Luciakova, D.; Belcher, J.; Tee, K. L.; Munro, A. W. Biological Diversity of Cytochrome P450 Redox Partner Systems. *Adv. Exp. Med. Biol.* **2015**, *851*, 299−317.
(96) Hussain, H. A.; Ward, J. M. Enhanced Heterologous Expression of Two *Streptomyces griseolus* Cytochrome P450s and *Streptomyces coelicolor* Ferredoxin Reductase as Potentially Efficient Hydroxylation Catalysts. *Appl. Environ. Microbiol.* **2003**, *69*, 373−382.
(97) Munro, A. W.; Leys, D. G.; McLean, K. J.; Marshall, K. R.; Ost, T. W. B.; Daff, S.; Miles, C. S.; Chapman, S. K.; Lysek, D. A.; Moser, C. C.; Page, C. C.; Dutton, P. L. P450BM3: the Very Model of a Modern Flavocytochrome. *Trends Biochem. Sci.* **2002**, *27*, 250−257.
(98) Roberts, G. A.; Grogan, G.; Greter, A.; Flitsch, S. L.; Turner, N. J. Identification of a New Class of Cytochrome P450 from a *Rhodococcus* sp. *J. Bacteriol.* **2002**, *184*, 3898−3908.
(99) Rimal, H.; Lee, S. W.; Lee, J. H.; Oh, T. J. Understanding of Real Alternative Redox Partner of *Streptomyces peucetius* DoxA: Prediction and Validation Using *in silico* and *in vitro* Analyses. *Arch. Biochem. Biophys.* **2015**, *585*, 64−74.

DOI: 10.1021/acscatal.8b02913
ACS Catal. 2018, 8, 9992−10003